Experimental and first-principles studies on superconductivity in noncentrosymmetric La_3Se_4

Moumita Naskar,[2] Soumen Ash,[3,1] Debendra Prasad Panda,[4] Chandan Kumar Vishwakarma,[2] Brajesh Kumar Mani,[2] A. Sundaresan,[4] and Ashok Kumar Ganguli[1,5,*]

[1]*Department of Chemistry, Indian Institute of Technology Delhi, New Delhi 110016, India*
[2]*Department of Physics, Indian Institute of Technology Delhi, New Delhi 110016, India*
[3]*Institute of Nano Science and Technology, Mohali 140306, India*
[4]*School of Advanced Materials and Chemistry and Physics of Materials Unit, Jawaharlal Nehru Centre for Advanced Scientific Research, Bangalore 560064, India*
[5]*Department of Materials Science and Engineering, Indian Institute of Technology Delhi, New Delhi 110016, India*

(Received 9 May 2021; revised 20 November 2021; accepted 3 January 2022; published 24 January 2022)

We report the synthesis and detailed characterization of superconducting La_3Se_4, with $T_c \sim 8.5 \pm 0.1$ K, using x-ray diffraction, electrical transport, magnetization, and heat capacity measurements. La_3Se_4 crystallizes in the noncentrosymmetric cubic Th_3P_4-type structure with space group $I\bar{4}3d$. Characteristic superconducting parameters such as the lower critical field, upper critical field, thermodynamic critical field, coherence length, penetration depth, and Ginzburg-Landau parameter have been determined. The specific heat jump at T_c, $\Delta C/\gamma T_c = 2.04 \pm 0.05$, exceeds the value for a weakly coupled BCS superconductor, and the electron-phonon coupling constant is found to be $\lambda_{ep} = 0.87 \pm 0.02$, suggesting superconductivity in La_3Se_4 is in the strong-coupling regime. The estimated upper critical field is well below the calculated Pauli limit, and the Maki parameter value ($\alpha < 1$) indicates that the superconducting upper critical field is dominated by orbital pair breaking. From density functional theory based first-principles simulations we observe the number of states at the Fermi energy is dominated mainly by d and f electrons of La. Furthermore, we observe band crossings along the high-symmetry k lines in the vicinity of the Fermi energy. These bands are observed to split due to the removal of spin degeneracy associated with spin-orbit coupling, with the splitting energy $E_{\mathrm{ASOC}} \approx 65$ meV.

DOI: 10.1103/PhysRevB.105.014513

I. INTRODUCTION

The discovery of superconductivity in materials lacking an inversion center has drawn attention to the understanding of the electronic structure and its relation to the mechanism of superconductivity [1–7]. The absence of inversion symmetry introduces antisymmetric spin-orbit coupling (ASOC) which lifts the original conduction electron spin degeneracy at the Fermi level, splitting it into two spin-ordered subsurfaces. This allows the admixture of spin-singlet and spin-triplet pairing states within the same orbital channel [1,8]. Noncentrosymmetric superconductors have attracted much interest since the discovery of superconductivity in Ce-based heavy-fermion superconductors such as $CePt_3Si$ [9], $CeRhSi_3$ [10], and $CeIrSi_3$ [11], as they offer a novel platform for unconventional superconductivity by favoring the pair-mixing mechanism. The other well-known examples of noncentrosymmetric superconductors are $Mg_{10}Ir_{19}B_{16}$ [12], $Li_2(Pt, Pd)_3B$ [13,14], and Mo_3Al_2C [15].

La_3Se_4 belongs to the family of intermetallic rare-earth chalcogenides, R_3X_4, where R is a rare-earth metal and X represents a chalcogenide element (S, Se, or Te). It was first reported by Meisel [16] and subsequently by Zachariasen in relation to Ce_2S_3 [17]. La_3Se_4 crystallizes in the noncentrosymmetric bcc crystal structure of Th_3P_4 type, with space group $I\bar{4}3d$. It was reported to be a superconductor with $T_c \sim 8.6$ K [18] and undergoes a cubic (space group: $I\bar{4}3d$) to tetragonal (space group: $I\bar{4}2d$) structural phase transformation below ~60–72 K [19,20]. Although there are some reports on superconductivity and the associated structural phase transition in La_3Se_4 [19–25], extensive study on the superconducting properties of this system is still required. In addition, the lack of inversion symmetry in the crystal structure opens the channel for a possible mixing of spin-singlet and spin-triplet states [26]. In the previous studies, however, there have been no comprehensive reports focusing on the possible pair-mixing scenario in La_3Se_4.

It can thus be inferred that there is a clear research gap in terms of the superconducting characteristics and the electronic structure of La_3Se_4. The aim of this study is to fill this research gap. During this study, we successfully synthesized polycrystalline La_3Se_4 using the solid-state reaction technique. Detailed measurements were carried out to study the electrical transport, magnetic, and thermal properties of La_3Se_4. We estimate both the normal-state properties, such as the Sommerfeld coefficient and density of states, and the characteristic superconducting parameters, such as the lower critical field, upper critical field, coherence length, penetration depth, thermodynamic critical field, and Ginzburg-Landau parameter. We also estimate the strength of the electron-phonon pairing in this material, and we find that La_3Se_4 exhibits a

*ashok@chemistry.iitd.ac.in

superconducting behavior in the strong-coupling limit. The effect of antisymmetric spin-orbit coupling in the electronic structure is examined from first-principles simulations. From our simulations, we observe band crossings in the vicinity of the Fermi energy. Each of these bands is found to split into two due to the removal of spin degeneracy after the spin-orbit coupling is switched on. Furthermore, from a detailed analysis of electronic structure, we observe that the bands in the vicinity of the Fermi energy are dominated by the mixed character of the d and f electrons of La.

II. EXPERIMENTAL AND SIMULATION DETAILS

Polycrystalline samples with a nominal composition of La_3Se_4 were synthesized by reacting La and Se (in elemental form). The stoichiometric amounts of reactants were mixed well, sealed in an evacuated quartz tube, and annealed at 1173 K for 24 h. The product was again ground, pelletized, and sintered at 1173 K for 24 h to achieve better phase homogeneity. The phase purity of the sample was verified with the powder x-ray diffraction technique using a Bruker D8 Advance diffractometer with Cu $K\alpha$ radiation. The structural refinement of powder x-ray diffraction data was carried out using the Rietveld method with the TOPAS software package [27]. The field-dependent and temperature-dependent magnetic measurements were carried out using a superconducting quantum interference device (SQUID; Quantum Design). A conventional four-probe technique was used for the transport studies. The data were collected for 2–300 K and magnetic fields up to 7 T using a physical property measurement system (PPMS; Quantum Design). The specific heat data were measured in the PPMS by using the time relaxation technique.

Fully relativistic first-principles simulations of the electronic structure were carried out using density functional theory as implemented in the Vienna Ab initio Simulation Package (VASP) [28–30]. The projector augmented-wave method [31,32] based plane wave basis with an energy cutoff of 500 eV was used in all the calculations. The effects of exchange correlation among electrons were incorporated using the generalized gradient approximation based Perdew-Burke-Ernzerhof pseudopotential. A convergence criterion of 1.0×10^{-8} eV was used for all self-consistent field calculations. For geometry optimization, all the structures were relaxed until the atomic forces decreased below 1.0×10^{-5} eV/Å. An optimized Monkhorst-Pack k mesh of $9 \times 9 \times 9$ was used in all the calculations.

III. RESULTS AND DISCUSSION

Figure 1(a) shows the Rietveld refinement of the room temperature powder x-ray diffraction pattern of La_3Se_4. It crystallizes in the Th_3P_4- type noncentrosymmetric cubic structure with space group $I\bar{4}3d$, and the lattice parameter is $a = 9.0381(2)$ Å. The details of the refined structural parameters are given in Table I. Figure 1(b) depicts the crystal structure of La_3Se_4, where La and Se ions occupy the 12a and 16c sites, respectively, and each La ion is coordinated by *eight* Se ions. Due to the polycrystalline nature of the sample, the measured physical properties are averaged over all the crystallographic directions. For a cubic crystal structure, however, this would not make a significant change in the measured physical parameters over different directions.

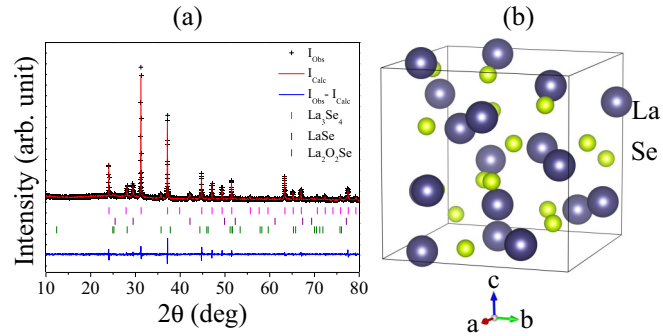

FIG. 1. (a) Rietveld refinement of room temperature powder x-ray diffraction data for polycrystalline La_3Se_4. Vertical bars indicate the allowed Bragg's reflections for La_3Se_4 and impurity phases. The blue line indicates the difference in the observed and fitted patterns. (b) Crystal structure of La_3Se_4.

Figure 2(a) shows the temperature dependence of the resistivity data studied under zero magnetic field. As is discernible from Fig. 2(a), a sharp superconducting transition is observed at $T_c \sim 8.5 \pm 0.1$ K with a transition width of $\Delta T_c \sim 1$ K. Superconductivity in La_3Se_4 is also characterized by the temperature-dependent DC magnetic susceptibility studied at an external magnetic field of 100 Oe, as shown in Fig. 2(b). Due to vortex pinning, the field-cooling signal is much smaller than the zero-field-cooling signal. The onset of diamagnetism occurs at $\sim 8 \pm 0.2$ K, which is slightly lower than the onset of the superconducting transition temperature observed in the

TABLE I. Structural, normal-state, and superconducting parameters of La_3Se_4 [space group: $I\bar{4}3d$; $a = 9.0381(2)$ Å] with their respective units.

Atom	Site	x	y	z	Occu.	B_{eq} (Å^2)
La	12a	0.375	0.0	0.25	1	2.9(1)
Se	16c	0.0749(5)	0.0749(5)	0.0749(5)	1	4.9(1)

Parameter	Value
T_c	8.5 ± 0.1 K
Θ_D	202.8 ± 0.5 K
$\Delta C/\gamma T_c$	2.04 ± 0.05
$N(E_F)$ (expt.)	5.8 ± 0.4 states eV^{-1} f.u.$^{-1}$
$N(E_F)$ (theory)	9.1 states eV^{-1} f.u.$^{-1}$
$N(E_F)$ (theory)(La deficient)	6.4 states eV^{-1} f.u.$^{-1}$
γ (expt.)	25.7 ± 1.28 mJ mol^{-1}K^{-2}
γ_{band}(theory)	21.46 mJ mol^{-1}K^{-2}
γ_{band} (theory)(La deficient)	15.16 mJ mol^{-1}K^{-2}
λ_{ep} (expt.)	0.87 ± 0.02
$\mu_0 H_{c1}(0)$	10.89 ± 0.03 Oe
$\mu_0 H_{c2}(0)$	13.24 ± 0.2 T
$\mu_0 H_c(0)$	528 ± 18 Oe
$\mu_0 H_P$	29.25 ± 0.2 T
$\xi_{GL}(0)$	4.98 ± 0.03 nm
$\lambda_{GL}(0)$	875.8 ± 1 nm
κ	175 ± 1
E_{ASOC}	65 meV

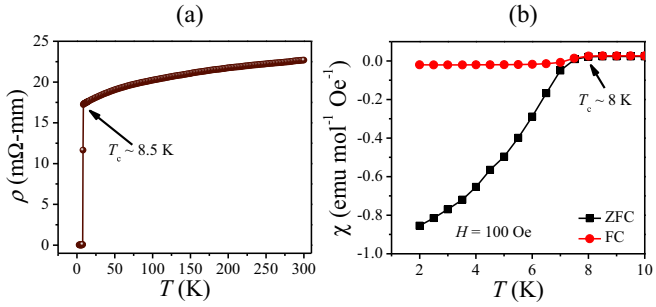

FIG. 2. (a) Resistivity as a function of temperature showing the superconducting transition for La_3Se_4 at 8.5 K. (b) The observed zero-field-cooling (ZFC) and field-cooling (FC) susceptibilities at an applied field of 100 Oe.

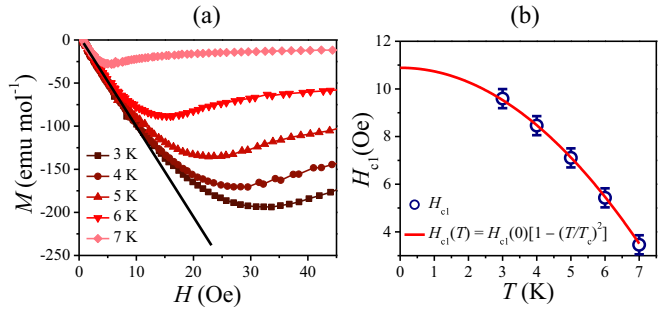

FIG. 4. (a) The zero-field-cooled magnetization $M(H)$ at different temperatures as a function of the magnetic field. (b) Fit of the H_{c1} data to the formula $H_{c1}(T) = H_{c1}(0)[1 - (T/T_c)^2]$ to extract the value of $\mu_0 H_{c1}(0)$.

transport measurement. The structural phase transition around 60–72 K that was reported earlier [19,25] is not observed in the resistivity and specific heat data for our sample. The reason may be a slight La deficiency in the stoichiometry of La_3Se_4 [25].

To characterize the superconductivity of La_3Se_4 further, temperature-dependent specific heat measurements were carried out at zero field and a magnetic field of 5 T, and the resulting data are shown in Fig. 3(a). As is discernible from Fig. 3(b), at zero field, the specific heat shows a jump at $T_c \sim 7.70 \pm 0.3$ K, determined using the isoentropic method, which confirms bulk superconductivity in La_3Se_4. At $\mu_0 H = 5$ T, the superconducting anomaly is, however, shifted to lower temperature, as shown in Fig. 3(a). The extension of the normal-state behavior towards the lower temperatures at higher magnetic fields allows the standard estimation of the Sommerfeld coefficient γ and the phonon specific-heat coefficient β by fitting the equation

$$C(T)/T = \gamma + \beta T^2. \tag{1}$$

Using our data for 5 T, we obtain $\gamma = 25.7 \pm 1.28$ mJ mol^{-1} K^{-2} and $\beta = 1.63 \pm 0.01$ mJ mol^{-1} K^{-4} from the fit shown by the red solid line in Fig. 3(a). Using the value of the specific heat jump at T_c from Fig. 3(b) along with γ, we find the value of $\Delta C/\gamma T_c$ to be 2.04 ± 0.05. This value

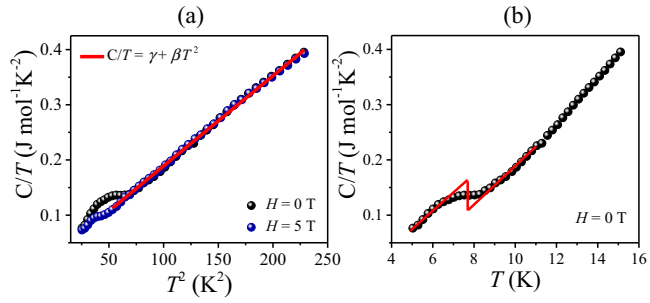

FIG. 3. (a) C/T vs T^2 data measured at $H = 0$ T and $H = 5$ T; the red solid line represents the fit to the equation $C/T = \gamma + \beta T^2$. (b) Temperature-dependent specific heat measured at $H = 0$ T, showing the bulk superconducting jump and isoentropic approach for obtaining T_c.

is larger than the BCS limit of 1.43 for a weakly coupled superconductor.

In a simple Debye model for the phonon contribution to the specific heat, the coefficient β is related to the Debye temperature Θ_D through the equation

$$\beta = \left(\frac{12}{5}\right) n\pi^4 R\Theta_D^{-3}, \tag{2}$$

where n is the number of atoms in the formula unit and R is the universal gas constant. Using the value of β, extracted from the specific heat data, $n = 7$ for La_3Se_4, and $R = 8.314$ J mol^{-1} K^{-1}, we obtain the value of $\Theta_D \approx 202.8 \pm 0.5$ K. Next, we determine the value of the electron-phonon coupling constant λ_{ep} using McMillan's formula [33],

$$\lambda_{ep} = \frac{1.04 + \mu^* \ln(\Theta_D/1.45T_c)}{(1 - 0.62\mu^*)\ln(\Theta_D/1.45T_c) - 1.04}, \tag{3}$$

where μ^* is the Coulomb pseudopotential of ≈0.13 for intermetallic superconductors. Using this value of μ^*, we obtain the value of $\lambda_{ep} \approx 0.87 \pm 0.02$. This considerable value of λ_{ep} in combination with the value for $\Delta C/\gamma T_c$, surpassing the BCS limit, indicates a strongly coupled superconductivity. Using the values of γ and λ_{ep}, we can calculate the density of states at the Fermi energy $N(E_F)$ using the relation $N(E_F) = 3\gamma/[\pi^2 k_B^2(1 + \lambda_{ep})]$, where k_B is the Boltzmann constant. We obtain $N(E_F) \approx 5.8 \pm 0.4$ states eV^{-1} f.u.$^{-1}$ from our experiment.

Next, we determine the lower critical field H_{c1} for La_3Se_4. For this we carried out field-dependent magnetization measurements at different temperatures; the data are shown in Fig. 4(a). As is evident from the trends in Fig. 4(a), with increasing applied magnetic field, the magnetization starts to deviate from the linear behavior, leading to a lower critical field for each isotherm. The values of H_{c1} obtained for each isotherm were then plotted as a function of temperature, as shown in the Fig. 4(b). The $H_{c1}(T)$ data show a parabolic nature and therefore are fitted to the quadratic temperature-dependent Ginzburg-Landau formula

$$H_{c1}(T) = H_{c1}(0)(1 - t^2), \tag{4}$$

where $t = T/T_c$, to extract the value of $\mu_0 H_{c1}(0)$. The corresponding fit is shown by the solid red line in Fig. 4(b). The value of $\mu_0 H_{c1}(0)$ extracted from the fit is 10.89 ± 0.03 Oe.

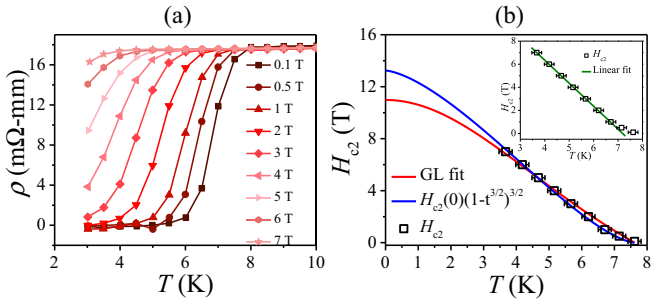

FIG. 5. (a) The superconducting transition under various magnetic fields. (b) The temperature dependence of the upper critical field extracted from the resistivity curves. The data are fitted by two different equations. The inset in (b) shows a linear fit (solid green line) with a slope of $dH_{c2}/dT = -2.02 \pm 0.02$ T/K.

To determine the upper critical field H_{c2} for La_3Se_4, we performed temperature-dependent resistivity measurements at different fields ranging from 0.1 to 7 T, as shown in Fig. 5(a). Using the value of the resistive onset temperature T_c^{onset} for different applied magnetic fields, the upper critical fields are plotted as a function of temperature in Fig. 5(b). As can be observed in Fig. 5(b), the temperature dependence of H_{c2} shows an upward-like feature near T_c. A similar upward-like nature for $H_{c2}(T)$ was also reported in the cases of $Nb_{0.18}Re_{0.82}$ [34], $PbTaSe_2$ [35], $PbTaS_2$ [36], MgB_2 [37], and borocarbide [38,39] superconductors. This behavior could be attributed to the multiband nature of the system [40,41]. Such phenomena can also be explained by the strong spin-orbit coupling model [42,43]. In the literature [34–36,38], this upward character of $H_{c2}(T)$ is well explained by the temperature-dependent formula

$$H_{c2}(T) = H_{c2}(0)(1 - t^{3/2})^{3/2}, \tag{5}$$

where $t = T/T_c$ [44–47]. Using this, we observed an excellent fit (shown by the blue line), with $R^2 = 0.997$, of our $H_{c2}(T)$ data and extracted the value of $\mu_0 H_{c2}(0) = 13.24 \pm 0.2$ T. This value of $\mu_0 H_{c2}(0)$ is larger than the value of 10.98 ± 0.2 T obtained from the fit (shown by the red line) using the generalized Ginzburg-Landau formula $H_{c2}(T) = H_{c2}(0)[(1 - t^2)/(1 + t^2)]$, where $t = T/T_c$. The reason for this is attributed to the better fit using the former expression. Since the value 13.24 ± 0.2 T is more reliable, in the calculations of other superconducting parameters we have used this value.

Using the value of 13.24 ± 0.2 T for $\mu_0 H_{c2}(0)$ in the Ginzburg-Landau formula, $\xi_{GL}(0) = [\Phi_0/2\pi H_{c2}(0)]^{1/2}$, with $\Phi_0 = h/2e$ (h is the Plank constant and e is the charge of the electron), we estimated the value of the coherence length $\xi_{GL}(0) = 4.98 \pm 0.03$ nm. The Ginzburg-Landau superconducting penetration depth λ_{GL}, calculated using the relation $\mu_0 H_{c1}(0) = (\Phi_0/4\pi\lambda_{GL}^2)\ln(\lambda_{GL}/\xi_{GL})$, is $\approx 875.8 \pm 1$ nm. For a superconductor, ξ_{GL} is a measure of the range to which superconducting order will extend in the bulk material, whereas λ_{GL} defines a characteristic length over which the magnetic field induced supercurrent reduces by a factor of e^{-1} from its surface value. The characteristic Ginzburg-Landau parameter $[\kappa = \lambda_{GL}(0)/\xi_{GL}(0)]$ is estimated to be $\kappa = 175 \pm 1$, which is larger than the limiting value of $1/\sqrt{2}$ for type-I superconductors, indicating La_3Se_4 is a type-II superconductor. We also estimated the value of the thermodynamic critical field, which provides a measure of the superconducting condensation energy, as $\mu_0 H_c(0) = 528 \pm 18$ Oe using the relation $H_{c1}(0)H_{c2}(0) = H_c^2 ln(\kappa)$.

There are two mechanisms to explain the Cooper pair breaking in a type-II superconductor due to the applied magnetic field: the orbital-limiting effect and the Pauli paramagnetic effect. In orbital pair breaking, the field-induced kinetic energy of a Cooper pair exceeds the superconducting condensation energy, whereas in the Pauli paramagnetic effect, the Zeeman splitting energy of electrons exceeds the superconducting condensation energy, and hence, the Cooper pair becomes unfavorable. The orbital critical field for a single-band, BCS-type superconductor is given by the Werthamer-Helfand-Hohenberg (WHH) formula [48],

$$H_{c2}^{\text{orb}} = -AT_c\left(\frac{dH_{c2}}{dT}\right)_{T=T_c}, \tag{6}$$

where A is 0.69 and 0.73 for the dirty and clean limits, respectively.

In our case, in the vicinity of T_c, the low-field $H_{c2}(T)$ data deviate from the WHH approximation due to the positive curvature and may not exhibit the intrinsic behavior of the system that to be considered for estimation of $\mu_0 H_{c2}^{\text{orb}}$. Therefore, for the purpose of comparison, we have used the WHH formalism by taking the slope in the high-field region from 1 to 7 T, where the data follow a significant linear dependence, rather than the initial slope in the low-field region near T_c. A similar approach was adapted for $PbTaSe_2$ [35], MgB_2 [37], RNi_2B_2C (R = Y, Lu) [39], and $Li_2(Pd_{1-x}Pt_x)_3B$ [49] to determine the orbital critical field. From the linear fit of the H_{c2} vs T data, shown in the inset in Fig. 5(b), the slope $dH_{c2}/dT = -2.02 \pm 0.02$ T/K was determined, and using $T_c = 8.5 \pm 0.1$ K, we estimated the orbital upper critical fields as $\mu_0 H_{c2}^{\text{orb}} = 11.85 \pm 0.3$ T and 12.53 ± 0.3 T for the dirty and clean limits, respectively.

Further, if we consider only the spin paramagnetic effect, the Pauli limiting upper critical field [50,51] is given by $H_P = \Delta/\sqrt{2}\mu_B$, where μ_B is the Bohr magneton and for a weakly coupled BCS superconductor $\Delta = 1.76 k_B T_c$. In the case of strongly coupled superconductivity, on the other hand, the H_P value is further enhanced according to the relation $H_P^{\text{str}} = H_P(1 + \lambda_{ep})$ [52]. Since our material is inferred to be a strongly coupled superconductor from the specific heat studies, H_P can be renormalized by the strength of the electron-phonon coupling. Using this relation, we estimate the Pauli paramagnetic limiting upper critical field $H_P^{\text{str}} = 29.25 \pm 0.2$ T.

Using the value of the orbital critical field and H_P, we can also determine the characteristic Maki parameter, expressed as $\alpha = \sqrt{2}H_{c2}^{\text{orb}}/H_P^{\text{str}}$ [53]. α provides a convenient measure for the relative strength of the orbital and spin pair breaking mechanisms. The values obtained for α are 0.57 ± 0.04 and 0.61 ± 0.04 for the dirty and clean limits, respectively. A value of α *less than* 1 indicates that the upper critical field in La_3Se_4 is dominated by the orbital depairing mechanism. If the upper critical field exceeds the Pauli limit, then the effect of Pauli pair breaking is non-negligible, and there could

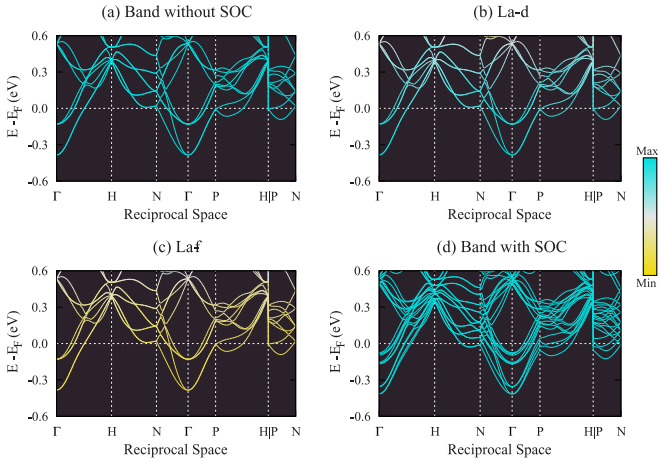

FIG. 6. The electronic band structure of La_3Se_4 (a) without and (d) with spin-orbit coupling. (b) and (c) The orbital-projected bands without SOC.

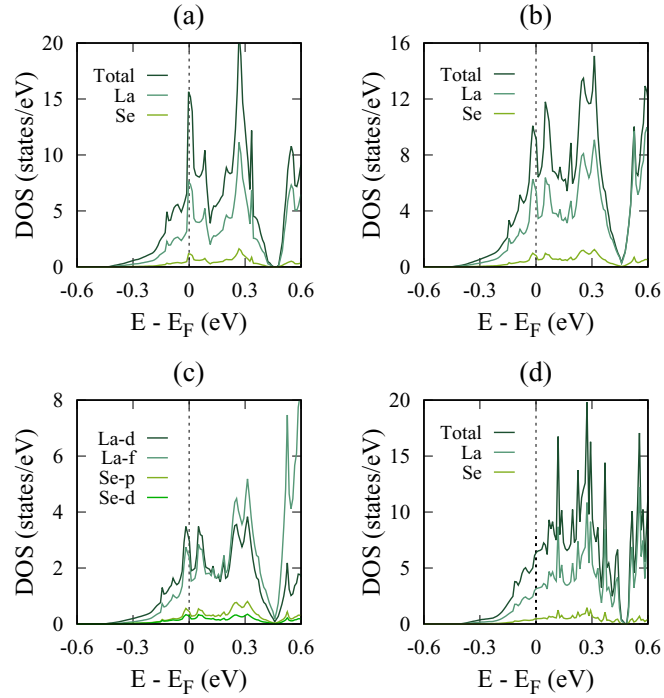

FIG. 7. The density of states and atom-projected density of states (a) without and (b) with spin-orbit coupling. (c) The orbital-projected density of states with spin-orbit coupling. (d) The density of states of 2.78% La-deficient La_3Se_4 with spin-orbit coupling.

be a substantial contribution of spin triplet components, suggesting a possible pair-mixing scenario due to the broken inversion symmetry. In our case, since the value of the upper critical field is comparable to the orbital critical field and is significantly smaller than the Pauli limit, the effect of Pauli pair breaking is inconsiderable, and hence, the possible pair-mixing scenario due to the broken inversion symmetry is not applicable to our system. The normal-state and superconducting parameters estimated from our measurements are provided in Table I.

To get further insight into the observed superconductivity in La_3Se_4 at low temperature, we examined the electronic structure from first-principles simulations. In Fig. 6, we show the electronic band structure of La_3Se_4 in the vicinity of the Fermi energy without [Fig. 6(a)] and with spin-orbit coupling [SOC; Fig. 6(d)]. And in Figs. 6(b) and 6(c) we show the orbital-projected bands of the d and f electrons of La, respectively. The bands around the Fermi energy are of mixed La d and f character, with the d contribution being slightly larger than the f contribution at the Fermi energy. As expected, the contribution from the f electrons starts dominating in the conduction band as we move away from the Fermi energy. There is a negligible contribution from Se, and therefore, it is not shown in this paper. Looking at the bands close to the Fermi energy in the absence of SOC, we observe band crossings along the Γ-H, Γ-N, Γ-P, P-H, and H-N k lines. As is discernible from Fig. 6(d), after SOC is switched on, each of these bands splits into two. The reason for this is attributed to the removal of spin degeneracy due to antisymmetric spin-orbit coupling. The antisymmetric spin-orbit splitting energy E_{ASOC} for La_3Se_4 is found to be ≈65 meV. The value of E_{ASOC} for La_3Se_4 from our simulation is close to the value obtained in another La-based noncentrosymmetric superconductor, $LaNiC_2$ (≈42 meV), where two-gap superconductivity is observed [54].

Figures 7(a) and 7(b) show the density of states (DOS) and atom-projected DOS without and with SOC, respectively. In Fig. 7(c) we show the orbital-projected DOS in the presence of SOC. As observed from Figs. 7(a) and 7(b), the Fermi energy lies at the local maximum of the DOS, leading to nonzero states at the Fermi energy. The dominant contribution at the Fermi energy is from La. One key observation for contributions from La is that, consistent with the band structure, although the d electrons provide the dominant contribution, the contribution from the f electrons is not negligible. This trend is consistent with the previous calculation [55] and could be attributed to the close energies of the d and f orbitals. Atomic Se provides a much smaller contribution than La, with the p electrons contributing the most at the Fermi energy. The total number of electronic states at the Fermi energy $N(E_F)$ with SOC is ≈9.1 states eV^{-1} $\mathrm{f.u.}^{-1}$, which is significantly large and favors the superconducting nature of the material. One important point to observe in the case of SOC is that $N(E_F)$ is reduced by ≈40% of its value for the case without SOC. The reason for this could be attributed to the shifts in the energies of the d and f orbitals.

The value of the Sommerfeld coefficient obtained using the relation $\gamma_{\mathrm{band}} = \frac{\pi^2}{3} k_B^2 N(E_F)$, within the framework of the lowest-order Sommerfeld expansion of electronic specific heat, is $\gamma_{\mathrm{band}} = 21.46$ mJ mol^{-1} K^{-2}. The comparable value, 25.7 mJ mol^{-1} K^{-2}, of the experimental γ indicates that there is no scope for the electron-phonon renormalization factor, $\gamma = \gamma_{\mathrm{band}}(1 + \lambda_{\mathrm{ep}})$. The reason for this discrepancy could be attributed to the slightly electron-deficient sample, possibly due to very small changes in the stoichiometry, used in the measurement. The structural phase transition (at ∼60–72 K [19,20]) in stoichiometric La_3Se_4 has been found to be very sensitive to the number of vacancies in the La sites [25]. Particularly, a vacancy concentration of $x = 0.015$ in $La_{3-x}Se_4$

is found to completely suppress the structural transition and, as a result, the crystal structure remains cubic down to the lowest studied temperature [25]. Such a small La deficiency is difficult to precisely detect from energy dispersive x-ray analysis or powder x-ray diffraction techniques. In our case, we did not find any evidence of a structural phase transition down to 2 K for the studied sample from the resistivity, magnetic susceptibility, and heat capacity measurements. This further indicates the presence of a slight La deficiency in our measured sample. To determine the amount of La deficiency in our sample we carried out a series of deficiency-dependent electronic structure calculations. In Fig. 7(d) we show the DOS for a 2.78% La-deficient structure in the presence of SOC. As we observe from Fig. 7(d), the introduction of La deficiency leads to a reduction of ∼30% in the value of $N(E_F)$ compared to that of the stoichiometric La_3Se_4. The value of $N(E_F)$, 6.4 states eV^{-1} $f.u.^{-1}$, for the deficient sample is comparatively closer to the experimental value, 5.8 ± 0.4 states eV^{-1} $f.u.^{-1}$, determined from the specific heat data. Similarly, the theoretically estimated value $\gamma_{\text{band}} = 15.16$ mJ mol^{-1} K^{-2} for the deficient structure can be substantially correlated to the experimental value of $\gamma = 25.7$ mJ mol^{-1} K^{-2} by the renormalization $\gamma = \gamma_{\text{band}}(1 + \lambda_{ep})$. These results suggest that there is possibly an ≈3% La deficiency present in our studied sample. A similar effect of deficiency on the DOS was reported in the cases of La_2C_3 [56] and (Nb/Ta)Ir_2B_2 [57] superconductors.

IV. CONCLUSIONS

In summary, we investigated the superconducting properties of La_3Se_4, which has the noncentrosymmetric Th_3P_4-type cubic structure. The superconductivity with $T_c = 8.5$ K was confirmed by our resistivity, magnetic, and specific heat measurements. From our measurements, we also extracted various normal-state and superconducting parameters which may be relevant for future experiments on La_3Se_4. Our specific heat measurements suggest that La_3Se_4 is a strongly coupled superconductor. The estimated upper critical field was found to be significantly lower than the calculated Pauli paramagnetic limit when strong spin-orbit coupling is considered, and the value of the Maki parameter ($\alpha < 1$) suggested that the upper critical field is dominated by the orbital depairing mechanism. The first-principles simulations showed a significantly large number of states at the Fermi energy, supporting the experimental results for superconductivity. We observed band crossings near the Fermi energy, where each of these bands splits due to the spin-orbit coupling. Besides the dominance of La d electrons in the Fermi level a significant contribution of La f electrons was also observed. The density of states at the Fermi level was found to be highly sensitive to the La deficiency in La_3Se_4. We found that a La deficiency of 2.78% reduces the value of $N(E_F)$ by 30% and is closer to the measured value. Based on our combined experimental plus theoretical study, we find that La_3Se_4 offers a promising platform in the area of superconductivity in materials without inversion symmetry.

ACKNOWLEDGMENTS

We thank CRF, IIT Delhi, for the SQUID facility. We thank Prof. S. Patnaik for the preliminary transport measurement. M.N. acknowledges IIT Delhi for a fellowship. S.A. acknowledges INST Mohali for a fellowship. C.K.V. acknowledges Council of Scientific & Industrial Research, India, for a senior research fellowship [Grant No. 09/086(1297)/2017-EMR-I]. A.K.G. thanks Science and Engineering Research Board-Department of Science & Technology, India, for financial support (Sanction No. EMR/2016/000156). Computational results are based on computations using the High Performance Computing cluster, Padum, at IIT Delhi.

[1] L. P. Gor'kov and E. I. Rashba, Phys. Rev. Lett. **87**, 037004 (2001).
[2] S. K. Yip, Phys. Rev. B **65**, 144508 (2002).
[3] P. A. Frigeri, D. F. Agterberg, A. Koga, and M. Sigrist, Phys. Rev. Lett. **92**, 097001 (2004).
[4] K. V. Samokhin, E. S. Zijlstra, and S. K. Bose, Phys. Rev. B **69**, 094514 (2004).
[5] S. Fujimoto, J. Phys. Soc. Jpn. **76**, 051008 (2007).
[6] M. Smidman, M. B. Salamon, H. Q. Yuan, and D. F. Agterberg, Rep. Prog. Phys. **80**, 036501 (2017).
[7] M. Naskar, P. K. Mishra, S. Ash, and A. K. Ganguli, Bull. Mater. Sci. **44**, 278 (2021).
[8] E. Bauer and M. Sigrist, *Non-centrosymmetric Superconductors: Introduction and Overview*, Lecture Notes in Physics Vol. 847 (Springer, Berlin, 2012).
[9] E. Bauer, G. Hilscher, H. Michor, C. Paul, E. W. Scheidt, A. Gribanov, Y. Seropegin, H. Noël, M. Sigrist, and P. Rogl, Phys. Rev. Lett. **92**, 027003 (2004).
[10] N. Kimura, K. Ito, K. Saitoh, Y. Umeda, H. Aoki, and T. Terashima, Phys. Rev. Lett. **95**, 247004 (2005).
[11] H. Mukuda, T. Fujii, T. Ohara, A. Harada, M. Yashima, Y. Kitaoka, Y. Okuda, R. Settai, and Y. Onuki, Phys. Rev. Lett. **100**, 107003 (2008).
[12] T. Klimczuk, Q. Xu, E. Morosan, J. D. Thompson, H. W. Zandbergen, and R. J. Cava, Phys. Rev. B **74**, 220502(R) (2006).
[13] M. Nishiyama, Y. Inada, and G.-Q. Zheng, Phys. Rev. Lett. **98**, 047002 (2007).
[14] H. Q. Yuan, D. F. Agterberg, N. Hayashi, P. Badica, D. Vandervelde, K. Togano, M. Sigrist, and M. B. Salamon, Phys. Rev. Lett. **97**, 017006 (2006).
[15] A. B. Karki, Y. M. Xiong, I. Vekhter, D. Browne, P. W. Adams, D. P. Young, K. R. Thomas, J. Y. Chan, H. Kim, and R. Prozorov, Phys. Rev. B **82**, 064512 (2010).
[16] K. Meisel, Z. Anorg. Allg. Chem. **240**, 300 (1939).
[17] W. H. Zachariasen, Acta Crystallogr. **2**, 57 (1949).

[18] R. M. Bozorth, F. Holtzberg, and S. Methfessel, Phys. Rev. Lett. **14**, 952 (1965).
[19] P. D. Dernier, E. Bucher, and L. D. Longinotti, J. Solid State Chem. **15**, 203 (1975).
[20] K. Westerholt, H. Bach, S. Methfessel, D. Ray, and S. Ghatak, Solid State Commun. **45**, 137 (1983).
[21] J. Sosnowski, Phys. Status Solidi B **72**, 403 (1975).
[22] P. E. Seiden, Phys. Rev. **168**, 403 (1968).
[23] R. Shelton, A. Moodenbaugh, P. Dernier, and B. Matthias, Mater. Res. Bull. **10**, 1111 (1975).
[24] F. Holtzberg, P. E. Seiden, and S. von Molnar, Phys. Rev. **168**, 408 (1968).
[25] K. Westerholt, F. Timmer, and H. Bach, Phys. Rev. B **32**, 2985 (1985).
[26] S. S. Saxena and P. Monthoux, Nature (London) **427**, 799 (2004).
[27] Bruker AXS, TOPAS 4.2, Karlsruhe, Germany, 2009.
[28] G. Kresse and J. Hafner, Phys. Rev. B **47**, 558 (1993).
[29] G. Kresse and J. Furthmüller, Phys. Rev. B **54**, 11169 (1996).
[30] G. Kresse and J. Furthmüller, Comput. Mater. Sci. **6**, 15 (1996).
[31] P. E. Blöchl, Phys. Rev. B **50**, 17953 (1994).
[32] G. Kresse and D. Joubert, Phys. Rev. B **59**, 1758 (1999).
[33] W. L. McMillan, Phys. Rev. **167**, 331 (1968).
[34] A. B. Karki, Y. M. Xiong, N. Haldolaarachchige, S. Stadler, I. Vekhter, P. W. Adams, D. P. Young, W. A. Phelan, and J. Y. Chan, Phys. Rev. B **83**, 144525 (2011).
[35] M. N. Ali, Q. D. Gibson, T. Klimczuk, and R. J. Cava, Phys. Rev. B **89**, 020505(R) (2014).
[36] J. J. Gao, J. G. Si, X. Luo, J. Yan, Z. Z. Jiang, W. Wang, C. Q. Xu, X. F. Xu, P. Tong, W. H. Song, X. B. Zhu, W. J. Lu, and Y. P. Sun, J. Phys. Chem. C **124**, 6349 (2020).
[37] Y. Takano, H. Takeya, H. Fujii, H. Kumakura, T. Hatano, K. Togano, H. Kito, and H. Ihara, Appl. Phys. Lett. **78**, 2914 (2001).
[38] M. D. Lan, J. C. Chang, K. T. Lu, C. Y. Lee, H. Y. Shih, and G. Y. Jeng, IEEE Trans. Appl. Supercond. **11**, 3607 (2001).
[39] K. D. D. Rathnayaka, A. K. Bhatnagar, A. Parasiris, D. G. Naugle, P. C. Canfield, and B. K. Cho, Phys. Rev. B **55**, 8506 (1997).
[40] A. Gurevich, Phys. Rev. B **67**, 184515 (2003).
[41] H. Lei, D. Graf, R. Hu, H. Ryu, E. S. Choi, S. W. Tozer, and C. Petrovic, Phys. Rev. B **85**, 094515 (2012).
[42] L. N. Bulaevskii, O. V. Dolgov, and M. O. Ptitsyn, Phys. Rev. B **38**, 11290 (1988).
[43] N. Kimura, K. Ito, H. Aoki, S. Uji, and T. Terashima, Phys. Rev. Lett. **98**, 197001 (2007).
[44] R. Micnas, J. Ranninger, and S. Robaszkiewicz, Rev. Mod. Phys. **62**, 113 (1990).
[45] A. S. Alexandrov, J. Ranninger, and S. Robaszkiewicz, Phys. Rev. B **33**, 4526 (1986).
[46] A. S. Alexandrov, Phys. Rev. B **48**, 10571 (1993).
[47] A. Alexandrov, Phys. C (Amsterdam, Neth.) **404**, 22 (2004).
[48] N. R. Werthamer, E. Helfand, and P. C. Hohenberg, Phys. Rev. **147**, 295 (1966).
[49] D. C. Peets, G. Eguchi, M. Kriener, S. Harada, Sk. Md. Shamsuzzamen, Y. Inada, G.-Q. Zheng, and Y. Maeno, Phys. Rev. B **84**, 054521 (2011).
[50] A. M. Clogston, Phys. Rev. Lett. **9**, 266 (1962).
[51] B. S. Chandrasekhar, Appl. Phys. Lett. **1**, 7 (1962).
[52] M. Schossmann and J. P. Carbotte, Phys. Rev. B **39**, 4210 (1989).
[53] K. Maki, Phys. Rev. **148**, 362 (1966).
[54] J. Chen, L. Jiao, J. L. Zhang, Y. Chen, L. Yang, M. Nicklas, F. Steglich, and H. Q. Yuan, New J. Phys. **15**, 053005 (2013).
[55] K. S. Fries and S. Steinberg, Chem. Mater. **30**, 2251 (2018).
[56] J. S. Kim, W. Xie, R. K. Kremer, V. Babizhetskyy, O. Jepsen, A. Simon, K. S. Ahn, B. Raquet, H. Rakoto, J.-M. Broto, and B. Ouladdiaf, Phys. Rev. B **76**, 014516 (2007).
[57] K. Górnicka, X. Gui, B. Wiendlocha, L. T. Nguyen, W. Xie, R. J. Cava, and T. Klimczuk, Adv. Funct. Mater. **31**, 2007960 (2021).